Robotica (2010) volume 28, pp. 539–547. © Cambridge University Press 2009
doi:10.1017/S0263574709990233

A new approach to the dynamic parameter identification of robotic manipulators

Zhongkai Qin*, Luc Baron and Lionel Birglen

Department of Mechanical Engineering, École Polytechnique, Montréal, Québec, Canada H3C 3A7

(Received in Final Form: May 22, 2009. First published online: June 24, 2009)

SUMMARY

This paper presents a novel systematic approach to identify the dynamic parameters of robotic manipulators. A sequential identification procedure is first proposed to deal with the difficulties usually encountered with standard approaches. An all-accelerometer inertial measurement unit (IMU) is also suggested to estimate the joint velocities and accelerations, which are traditionally obtained by differentiating the joint positions. The IMU kinematics and the computation method for estimation joint motion from IMUs are provided. The proposed method yields promising results in improving the identification precision compared to conventional methods. Finally, practical experiments are conducted to validate the theoretical results.

KEYWORDS: Robot dynamics; Dynamic identification; Robotic manipulator; Serial robot; Inertial measurement.

1. Introduction

The dynamic model of a robot is essential in simulating its motion, implementing a model-based control strategy and developing accurate path planning algorithms.[15,18] Although the equations of motion can be derived by using either Newton–Euler or Lagrange methods with the help of a symbolic computation software, the actual inertial and frictional dynamic parameters of the mechanical system are not easily quantifiable. Computing their values from a CAD model is only approximative because of the numerous components with irregular shapes and unmodeled parts made of a variety of materials. Moreover, disassembling the robot to estimate the inertial parameters of its individual components by pendulum tests or Mass Properties Measurement Instruments[1] is also impractical in general. In the late 1980s, significant contributions were made to the identification of dynamic parameters via the standard least square technique.[5,9,16] This approach relies on formulating the dynamic model of the manipulator in a form linear with respect to the parameters to be identified. Experiments are then conducted to collect data of generalized forces and joint motions while the manipulator executes a trajectory. Using these measurements, the dynamic parameters are estimated using linear regression techniques. When conducting such experiments, it is essential to design an "exciting" trajectory which guarantees accurate parameter estimation in the presence of disturbances such as measurement noise.[1,7,13,17]

To date, the dynamic identification of robotic systems is far from a solved problem. There are several hindrances that prevent one from obtaining a satisfactory estimation. The first difficulty arises from an unreliable account of friction effects, which are usually significant. With nondirect-drive robots, an average of 25 % of the driving torque supplied by the actuators is used to overcome friction.[4] Friction forces depend on the mechanical construction of each drive, the lubrication conditions, the type of contact between the parts, and the magnitude of the relative velocity between contacts.[11] Moreover, friction forces also depend on the forces and moments in the components, which are complex functions of time. Therefore, the joint friction forces exhibit highly nonlinear characteristics and are usually extremely difficult to model. In practice, however, a simple model is usually considered to account for joint friction. This model is however often inaccurate and sometimes problematic.[12] Second, with the classical identification method, the computation of joint velocities and accelerations through differentiation of the (noisy) joint position signals yields significant errors into the identification process.[10,19] Third, the difficulty in the general approach proposed in the literature and briefly recalled in Section 2 is that for complicated dynamic models it requires the computation of the generalized inverse of a very large matrix (i.e., the *regressor*). Trying to identify a large number of parameters simultaneously with this method is prone to generate numerical errors. Finally, planning the exciting trajectories for a complex robotic system is a challenging task with the growing number of variables.[8] Thus, the difficulties arising from modeling, trajectory planning, and identification processes might result in unreliable results.

In this paper, a systematic approach is proposed to overcome the aforementioned difficulties. In this approach, dynamic parameters are identified sequentially: joint friction models are initially obtained; then, gravity parameters are identified; finally, the other parameters are estimated. Therefore, the dynamic parameters are identified in three steps using a reduced amount of data and complexity at each step. Moreover, inertial measurement unit (IMUs) are shown to allow for a more precise estimation of the joint velocities and accelerations than the numerical differentiation technique.

* Corresponding author. E-mail: zhongkai.qin@polymtl.ca

2. Parameter Identification

2.1. General procedure

To identify dynamic parameters, obtaining the dynamic model in close form is the first step. Lagrangian or Newton–Euler formulation can be used to this aim. A symbolic computation software is generally desirable to carry out the manipulations efficiently and reliably. Without any loss of generality, the dynamic equation for a manipulator can be written as

$$\boldsymbol{\tau} = \mathbf{D}(\mathbf{q})\ddot{\mathbf{q}} + \mathbf{C}(\mathbf{q}, \dot{\mathbf{q}})\dot{\mathbf{q}} + \mathbf{G}(\mathbf{q}) + \boldsymbol{\tau}_f, \tag{1}$$

where $\mathbf{D}(\mathbf{q})$ is called the *inertia matrix*, $\mathbf{C}(\mathbf{q}, \dot{\mathbf{q}})$ consists of centrifugal and Coriolis terms, $\mathbf{G}(\mathbf{q})$ accounts for gravity terms, and $\boldsymbol{\tau}_f$ models friction effects. Joint positions, velocities, accelerations and torques are respectively denoted by $\mathbf{q} = [\theta_1, \ldots, \theta_n]^T$, $\dot{\mathbf{q}} = [\dot{\theta}_1, \ldots, \dot{\theta}_n]^T$, $\ddot{\mathbf{q}} = [\ddot{\theta}_1, \ldots, \ddot{\theta}_n]^T$, and $\boldsymbol{\tau} = [\tau_1, \ldots, \tau_n]^T$, with a n degree-of-freedom (DOF) manipulator. Equation (1) contains various parameters. First, there are the manipulator geometric parameters. Usually the *Denavit–Hartenberg* convention is used, which consists of link lengths, offsets, and relative orientations of joint axes. Second, there are the inertial parameters, which, for the ith link, can be defined by the vector

$$\boldsymbol{\iota}_i = [m_i \; m_i r_i^x \; m_i r_i^y \; m_i r_i^z \; I_i^{xx} \; I_i^{xy} \; I_i^{xz} \; I_i^{yy} \; I_i^{yz} \; I_i^{zz}]^T,$$

where m_i is the mass of this link; $m_i r_i^x$, $m_i r_i^y$, and $m_i r_i^z$ are the Cartesian components of the first-order mass moment; I_i^{xx}, I_i^{xy}, I_i^{xz}, I_i^{yy}, I_i^{yz}, and I_i^{zz} are the components of the associated inertia tensor.

Next, there are friction terms. Usually, a mathematical model including the Coulomb and viscous coefficients is used to model friction. However, this model is not always satisfactory due to the reasons discussed in the introduction. Therefore, this paper proposes a new and more general method to model joint friction as detailed in Section 2.2.1.

Finally, the rotor inertia of the actuator requires a special attention. The latter, including the inertia of the transmission, is usually replaced by an equivalent inertia which is added to the link inertia, namely,

$$I_i^{zz} = I_{l,i}^{zz} + N_i^2 I_{m,i}, \tag{2}$$

where $I_{l,i}^{zz}$ is the inertia of the ith link around the associated joint axis, $I_{m,i}$ is the rotor inertia of this joint axis, and N_i is the transmission ratio of its reduction stage. However, this simplification is in fact improper,[17] because the inertial force of the rotor only depends on the angular acceleration of its joint, but that of the link itself also depends on angular accelerations of both the joint considered and all the previous joints. To include exact influence of these rotor inertias, they have to be regarded as a separate set of parameters in the model. Fortunately, the values of the rotor inertias are usually provided by the manufacturers and therefore have not to be identified. Taking all relevant parameters into account, the dynamic parameters associated with the ith link is defined as a 11th-dimensional vector, namely,

$$\boldsymbol{\eta}_i = \begin{bmatrix} \boldsymbol{\iota}_i \\ I_{m,i} \end{bmatrix}.$$

An important property of Eq. (1) is that it can be formulated linearly with respect to the dynamic parameters if the inertial tensor of each link is expressed relatively to the origin of its attached frame.[9] Using this technique, one obtains

$$\boldsymbol{\tau} = \mathbf{K}(\mathbf{q}, \dot{\mathbf{q}}, \ddot{\mathbf{q}})\boldsymbol{\phi} + \boldsymbol{\tau}_f, \tag{3}$$

where $\mathbf{K}(\mathbf{q}, \dot{\mathbf{q}}, \ddot{\mathbf{q}})$ is an $n \times 11n$ matrix, while $\boldsymbol{\phi} = [\boldsymbol{\eta}_1^T \; \ldots \; \boldsymbol{\eta}_n^T]^T$, and $\boldsymbol{\tau}_f = [\tau_{f,1}, \ldots, \tau_{f,n}]^T$. In fact, not all parameters in $\boldsymbol{\phi}$ contribute to the joint torques. As an example, the first link of many common robot architectures only rotates about a vertical axis. In this case, the only dynamic parameter of the link influencing the joint torque is its moment of inertia about this vertical axis. Therefore, many dynamic parameters can actually be discarded from Eq. (3). Furthermore, the remaining dynamic parameters must be regrouped in order to eliminate linear dependencies in $\mathbf{K}$ before using least square (LS) estimation. Eventually, the vector $\boldsymbol{\phi}$ can be replaced by a vector of *base parameters* $\boldsymbol{\pi}$, and the matrix $\mathbf{K}$ can be replaced by the corresponding reduced matrix $\mathbf{H}$ without losing any information from a dynamic perspective. Thus, one obtains

$$\boldsymbol{\tau}' = \mathbf{H}(\mathbf{q}, \dot{\mathbf{q}}, \ddot{\mathbf{q}})\boldsymbol{\pi}, \tag{4}$$

where $\boldsymbol{\tau}' = \boldsymbol{\tau} - \boldsymbol{\tau}_f$ and $\boldsymbol{\pi} = [\pi_1 \; \pi_2 \; \ldots \; \pi_b]^T$ with ($b \leq 11n$). A method to determine the base parameters for common serial manipulators whose successive axes are perpendicular or parallel is proposed in refs. [6, 8].

With conventional methods, the base parameters $\boldsymbol{\pi}$ are identified simultaneously by a LS estimation technique. To this purpose, data of joint positions, velocities, accelerations and torques are recorded w times during a trajectory executed by the manipulator (with $wn > b$). Using recorded data, Eq. (4) is written for each time sample and assembled into

$$\boldsymbol{\Gamma} = \begin{bmatrix} \boldsymbol{\tau}'_1 \\ \boldsymbol{\tau}'_2 \\ \vdots \\ \boldsymbol{\tau}'_w \end{bmatrix} = \begin{bmatrix} \mathbf{H}_1 \\ \mathbf{H}_2 \\ \vdots \\ \mathbf{H}_w \end{bmatrix} \boldsymbol{\pi} = \boldsymbol{\Phi}(\mathbf{H})\boldsymbol{\pi}, \tag{5}$$

where $\boldsymbol{\Phi}(\mathbf{H})$ is called a regressor. Then, $\boldsymbol{\pi}$ can be estimated by

$$\hat{\boldsymbol{\pi}} = (\boldsymbol{\Phi}^T\boldsymbol{\Phi})^{-1}\boldsymbol{\Phi}^T\boldsymbol{\Gamma} = \boldsymbol{\Phi}^I\boldsymbol{\Gamma}, \tag{6}$$

where $\hat{\boldsymbol{\pi}}$ is the LS estimate of the true value $\boldsymbol{\pi}$, and $\boldsymbol{\Phi}^I$ is the pseudo-inverse of $\boldsymbol{\Phi}$. Of course, the numerical computation of $\hat{\boldsymbol{\pi}}$ is difficult due to the (generally) huge dimensions of $\boldsymbol{\Phi}$.

2.2. Sequential identification

2.2.1. Modeling of joint friction. In general, friction torque is considered as a nonlinear discontinuous function of joint

https://doi.org/10.1017/S0263574709990233 Published online by Cambridge University Press

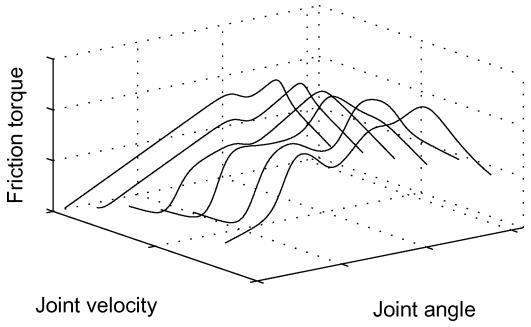

Fig. 1. Joint friction torque with respect to joint positions and velocities.

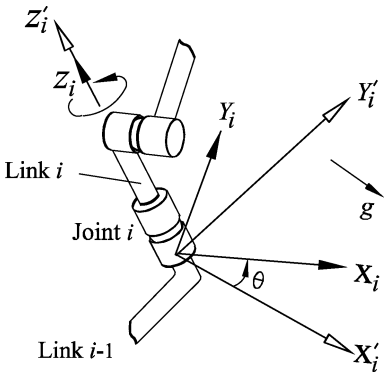

Fig. 2. ith joint in an arbitrary orientation.

velocity including Coulomb and viscous effects. However, friction in robotic joints also depends on stiction, asymmetries, and downward bends.[3] In this paper, a m-order polynomial model in terms of the joint positions and velocities is used to account for some of these factors, i.e., one has,

$$\tau_{f,i} = \sum_{j=0}^{m} c_j(\dot{\theta})\theta^j. \tag{7}$$

An experimental procedure can be carried out to identify the parameters of this friction model, namely the polynomial coefficients c_j. First, the joint friction is obtained as a function of joint position at different joint velocities as illustrated in Fig. 1. Then a m-order polynomial can be used to fit the friction torque data at a constant velocity $\dot{\theta}_j$, i.e.,

$$\tau_{f,i}(j) = c_0^*(\dot{\theta}_j) + \theta c_1^*(\dot{\theta}_j) + \cdots + \theta^m c_m^*(\dot{\theta}_j), \tag{8}$$

where $c_j^*(\dot{\theta}_j)$ with j from 0 to m are the coefficients numerically obtained (they are different from those used in Eq. (7)). One can repeat this procedure for n different velocities to obtain a vector representation, i.e.,

$$\boldsymbol{\tau}_{f,i} = \mathbf{c}_0^* + \theta \mathbf{c}_1^* + \cdots + \theta^m \mathbf{c}_m^*. \tag{9}$$

In turn, the elements in $\mathbf{c}_j^*$ can be used to compute a l-order polynomial approximating these coefficients over the range considered, namely,

$$c_j = \sum_{r=0}^{l} d_{j,r}\dot{\theta}^r, \tag{10}$$

and one obtains the joint friction model described in Eq. (7). In addition, m and l can be increased according to the complexity of the friction profile until the following criterion is met, i.e.,

$$\max_{ws}\left(\left|\frac{\tau_{f,i} - \tau_{d,i}}{\tau_{d,i}}\right|\right) \leq \beta, \tag{11}$$

where $\tau_{d,i}$ is the data of the measured friction torque, β is a threshold value, and ws is the workspace in position and velocity considered. Equation (11) measures how well the obtained friction model fits the experimental data. It should be noted that this equation becomes numerically ill-conditioned as $\tau_{d,i}$ approaches zero. In this case, the criterion can be revised to another form, e.g., without the denominator in the left side of Eq. (11).

2.2.2. Identification of joint friction. In our sequential identification process, friction models for each joint of the robot are constructed one by one. To illustrate this process, a general case, where the axis of the ith joint (assumed to be revolute) is skew with respect to the gravity vector $\mathbf{g}$, is illustrated in Fig. 2. It is desired to model the friction acting on this joint using the methodology presented in Section 2.2.1. All the other joints of the robot are considered locked. In this situation, gravity effects have to be removed in order to identify joint friction. A frame i' $(X_i' Y_i' Z_i')$ is rigidly attached to link $i-1$ and coincides with the rotating link frame i $(X_i Y_i Z_i)$ when the joint angle θ is zero. The first-order mass moment of the structure starting from this joint to the last body of the robot is noted $\boldsymbol{\xi} = [\zeta\rho_x \ \zeta\rho_y \ \zeta\rho_y]^T$ expressed in the frame i, where ζ denotes the mass of the structure and ρ_x, ρ_y, ρ_z are the coordinates of its center of mass. When this joint is rotated while the other joints are locked, the gravity torque exerted on the joint is

$$\tau_p = \mathbf{e}_z^T(\mathbf{g} \times \boldsymbol{\xi}) = \mathbf{a}^T \mathbf{p}_\xi, \tag{12}$$

with $\mathbf{e}_z = [0\,0\,1]^T$, $\mathbf{g}$ is the vector of gravitational acceleration with respect to frame i', and

$$\mathbf{a} = \begin{bmatrix} \mathbf{g}^T\mathbf{e}_x \sin\theta - \mathbf{g}^T\mathbf{e}_y \cos\theta \\ \mathbf{g}^T\mathbf{e}_x \cos\theta + \mathbf{g}^T\mathbf{e}_y \sin\theta \end{bmatrix}, \tag{13}$$

$$\mathbf{p}_\xi = \begin{bmatrix} \zeta\rho_x \\ \zeta\rho_y \end{bmatrix}, \tag{14}$$

where $\mathbf{e}_x = [1\,0\,0]^T$ and $\mathbf{e}_y = [0\,1\,0]^T$.

The joint i is then rotated with a constant velocity (hence, inertial forces are zero) in the following two tests: #1) from θ_{ini} to θ_{fin}; #2) from θ_{fin} to θ_{ini}, as illustrated in Fig. 3. In test #1, the joint torque required to drive the load is $\tau_1 = \tau_p + \tau_f$. Whereas, in test #2, the joint torque becomes $\tau_2 = \tau_p - \tau_f$. Using τ_1 and τ_2, it is trivial to obtain the torque due to gravity:

$$\tau_p = \frac{\tau_1 + \tau_2}{2}. \tag{15}$$

https://doi.org/10.1017/S0263574709990233 Published online by Cambridge University Press

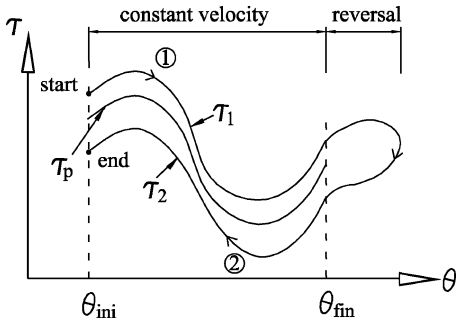

Fig. 3. Gravity torque estimation.

Thereupon, τ_p is known at each time sample and can be substituted into Eq. (12). Using LS estimation, one can identify $\mathbf{p}_\xi$. It should be noted that the purpose of identifying $\mathbf{p}_\xi$ is solely to remove gravity effect caused by $\boldsymbol{\xi}$; this procedure has nothing to do with the identification of gravity parameters discussed in Section 2.2.3. Moreover, the direction independence of the joint friction is assumed in the estimation of τ_p of Eq. (15).

Now the identification of joint friction can be handled. The joint is controlled to follow different trapezoidal velocity profiles in many trials with different values in the constant part of the profile. During each trial, the joint angles and torques are recorded. In these tests, τ_p can be computed by Eq. (12) with the identified value of $\mathbf{p}_\xi$. The joint friction torques are thereupon easily calculated by the following equation:

$$\tau_f = \pm(\tau_i - \tau_p), \tag{16}$$

where τ_i denotes the joint torque.

With the data of joint angles, velocities and friction torques, the procedure developed in Section 2.2.1 is used to obtain the friction model for the ith joint. Eventually, one can construct friction models for all the joints by repeating the proposed procedure sequentially. Thereupon, the friction torques can be predicted with these models in further steps of the parameter identification process.

2.2.3. Gravity parameters. The next step is to identify gravity parameters. To this purpose, Eq. (4) can be reformulated into

$$\boldsymbol{\tau}' = \begin{bmatrix} \mathbf{H}_g & \mathbf{H}_r \end{bmatrix} \begin{bmatrix} \boldsymbol{\pi}_g \\ \boldsymbol{\pi}_r \end{bmatrix}, \tag{17}$$

where $\boldsymbol{\pi}_g$ is a vector of the parameters in $\boldsymbol{\pi}$ associated with gravity effects, and $\boldsymbol{\pi}_r$ is the vector of all other parameters. Again, if one joint is rotating with constant velocity while all the others are locked, only the forces associated with gravity and friction play a role in the dynamic model. Therefore, Eq. (4) becomes

$$\boldsymbol{\tau}' = \boldsymbol{\tau}_g = \mathbf{H}_g \boldsymbol{\pi}_g. \tag{18}$$

Using single joint motions (with constant velocities) successively, e.g., from the last to the first joint and varying the configuration of the joints locked, identifying $\boldsymbol{\pi}_g$ can be reduced to a LS estimation problem again similar to Eq. (6), i.e.,

$$\boldsymbol{\Gamma}(\boldsymbol{\tau}_g) = \boldsymbol{\Phi}(\mathbf{H}_g)\boldsymbol{\pi}_g. \tag{19}$$

$\boldsymbol{\Phi}(\mathbf{H}_g)$ should have a small condition number to yield robust estimates of $\boldsymbol{\pi}_g$.[7] Therefore, prior to actual experiments, an optimization regarding the angles of locked joints can be performed to decrease the condition number of $\boldsymbol{\Phi}(\mathbf{H}_g)$ to the smallest possible value. It can be done by minimizing the cost function

$$f(\mathbf{q}(t)) = \text{cond}(\boldsymbol{\Phi}(\mathbf{H}_g)), \tag{20}$$

subject to

$$|\theta_i(t)| \le \theta_{i,max}\ , \tag{21}$$

where $\theta_{i,max}$ represents the ith joint limit and the operator "cond" denotes the condition number of a matrix.

It has been discussed previously that the identification of $\mathbf{p}_\xi$ differs from the identification of $\boldsymbol{\pi}_g$. However, the obtained data for τ_p in Section 2.2.2 can be reused and substituted into Eq. (19) for the identification of $\boldsymbol{\pi}_g$.

2.2.4. Inertial parameters. To identify $\boldsymbol{\pi}_r$, only a minimum number of axes are actuated to collect data in order to reduce the complexity of the experiment. To have some insights on the number of axes required to undergo motions, let us consider the detailed expression of Eq. (1), namely,

$$\tau_k = \sum_{j=1}^{n} d_{kj}\ddot{q}_j + \sum_{j=1}^{n} c_{kj}\dot{q}_j + g_k(\mathbf{q}) + \tau_{f,k} \quad \text{for } k = 1, \ldots, n, \tag{22}$$

where τ_k denotes the actuation torque of joint k, d_{kj} is the (k, j)th component of the $n \times n$ inertia matrix $\mathbf{D}(\mathbf{q})$, g_k is the gravity term, $\tau_{f,k}$ is the friction torque, and

$$c_{kj} \triangleq \sum_{i=1}^{n} \frac{1}{2}\left(\frac{\partial d_{kj}}{\partial q_j} + \frac{\partial d_{ki}}{\partial q_j} - \frac{\partial d_{ij}}{\partial q_i}\right)\dot{q}_i. \tag{23}$$

Inspecting Eq. (23), one can conclude that the elements of $\mathbf{C}(\mathbf{q}, \dot{\mathbf{q}})$ are functions of the parameters of the inertial matrix. Hence, the dynamic parameters appearing in $\mathbf{C}(\mathbf{q}, \dot{\mathbf{q}})$ are also found in $\mathbf{D}(\mathbf{q})$. When only joint k is actuated while the other are locked, Eq. (22) becomes

$$\tau_k = d_{kk}(\mathbf{q})\ddot{q}_k + c_{kk}(\mathbf{q})\dot{q}_k + g_k(\mathbf{q}) + \tau_{f,k}. \tag{24}$$

It is worth noting that in Eq. (24) the second term $c_{kk}\dot{q}_k = \frac{1}{2}\frac{\partial d_{kk}}{\partial q_k}\dot{q}_k^2$ should vanish since the centrifugal force is always perpendicular to the axis rotated. Thus, one has

$$\tau_k = d_{kk}\ddot{q}_k + g_k + \tau_{f,k}. \tag{25}$$

Only the parameters in the diagonal elements of the inertia matrix together with the gravity and friction terms appear in Eq. (25). The off-diagonal elements of the inertial matrix

https://doi.org/10.1017/S0263574709990233 Published online by Cambridge University Press

are not present and therefore cannot be identified with this method. Hence, solely moving one axis is not sufficient to completely identify the dynamic parameters. If, at each time, two axes are actuated and using different combination of joints successively, all the parameters in $\boldsymbol{\pi}_r$ will appear in the equations of motion. Then, a LS technique can be again setup to estimate $\boldsymbol{\pi}_r$ with

$$\boldsymbol{\Gamma} = \boldsymbol{\Phi}(\mathbf{H}_r)\boldsymbol{\pi}_r. \tag{26}$$

It is not necessary to use all the possible combinations (e.g., $C_6^2 = 15$ in case of a six-DOF serial robot) of any two joints for identifying $\boldsymbol{\pi}_r$. It is sufficient to take the number of combinations required for $\boldsymbol{\Phi}(\mathbf{H}_r)$ to have full rank. For instance, it is possible to only move the first joint of a three-joint planar manipulator while changing the configurations of the other two joints to yield $\boldsymbol{\Phi}(\mathbf{H}_r)$ full rank.

3. Joint Motion Estimation by IMUs

An IMU is the main component of the guidance system used in vehicles, aircrafts and satellites. Most of current IMUs are based on accelerometers and gyroscopes to sense respectively the linear acceleration and the angular velocity. These data are thereupon acquired by the controller of the guidance system, calculating the navigation parameters, i.e., the linear and angular velocities of the vehicle, and subsequently, its coordinates. The authors proposed the design of all-accelerometer IMUs to improve robustness of these computations.[14] In the sequential identification scheme proposed in this paper, two axes of an n $(n \geq 6)$-DOF manipulator are required to move simultaneously. In order to obtain accurate velocity and acceleration data for these two joints, the robot can be equipped with two IMUs. Initially, some necessary concepts regarding manipulator kinematics must be introduced in order to implement these two IMUs.

To describe the location and orientation of each link relative to its neighbors, a frame i is attached to the ith link as shown in Fig. 2. The rotation between two adjacent frames i and $i+1$ can be described using the rotation matrix

$$ {}^{i}_{i+1}\mathbf{Q} = \begin{bmatrix} \mathrm{c}_{\theta_{i+1}} & -\mathrm{s}_{\theta_{i+1}} & 0 \\ \mathrm{s}_{\theta_{i+1}}\mathrm{c}_{\alpha_i} & \mathrm{c}_{\theta_{i+1}}\mathrm{c}_{\alpha_i} & -\mathrm{s}_{\alpha_i} \\ \mathrm{s}_{\theta_{i+1}}\mathrm{s}_{\alpha_i} & \mathrm{c}_{\theta_{i+1}}\mathrm{s}_{\alpha_i} & \mathrm{c}_{\alpha_i} \end{bmatrix}, \tag{27}$$

where θ_{i+1} is the joint angle and α_i is the *Denavit–Hartenberg* parameter describing the angle between the Z-axes of respectively frames i and $i+1$. Moreover, the rotation between frame i and j can be expressed as the product of each intermediate rotation matrices, namely,

$$ {}^{i}_{j}\mathbf{Q} = {}^{i}_{i+1}\mathbf{Q}\,{}^{i+1}_{i+2}\mathbf{Q}\cdots{}^{j-1}_{j}\mathbf{Q}. \tag{28}$$

Two IMUs (a and b) are used to estimate joint velocities and accelerations when the m and l $(m < l)$ joints are rotating simultaneously. As illustrated in Fig. 4, IMUa is attached somewhere between joint m and joint l, whereas IMUb is fixed to the end-effector. The reasons for this arrangement are: IMUa has to be placed after joint m in order to estimate its motion; the motion of any joint between the end-effector and the joint m can be conveniently estimated with the placement of IMUb in the end-effector. First, let us consider estimating the motion of joint m by IMUa. Due to this motion, IMUa is subjected to an angular acceleration $\dot{\boldsymbol{\omega}}_a = [\dot{\omega}_{a,1}\ \dot{\omega}_{a,2}\ \dot{\omega}_{a,3}]^T$ computed from the outputs of IMUa. Since the joints before m are locked, the direction of $\dot{\boldsymbol{\omega}}_a$ is invariant, i.e.,

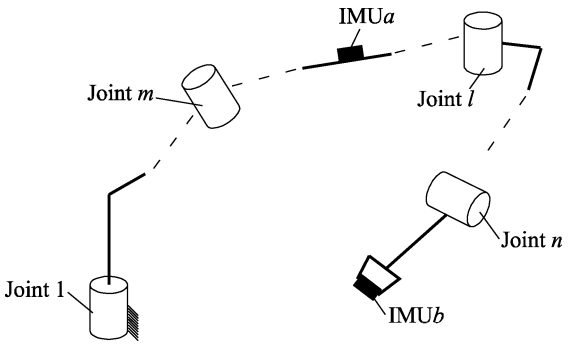

Fig. 4. IMU implementation.

$$\mathbf{a} \equiv [a_1\ a_2\ a_3]^T = \frac{1}{\|\dot{\boldsymbol{\omega}}_a\|}[\dot{\omega}_{a,1}\ \dot{\omega}_{a,2}\ \dot{\omega}_{a,3}]^T. \tag{29}$$

In fact, $\mathbf{a}$ is the direction vector of the joint axis expressed in the IMU frame. If joint m is driven with an acceleration $\ddot{\theta}_m^*$, the corresponding angular acceleration of IMUa is denoted $\dot{\boldsymbol{\omega}}_a^* = [\dot{\omega}_{a,1}^*\ \dot{\omega}_{a,2}^*\ \dot{\omega}_{a,3}^*]^T$. Subsequently, any future joint accelerations can be estimated as

$$\ddot{\theta}_m = \frac{\ddot{\theta}_m^*}{3}\sum_{i=1}^{3}\frac{\dot{\omega}_{a,i}}{\dot{\omega}_{a,i}^*}. \tag{30}$$

Similarly, the joint velocity can be determined as

$$\dot{\theta}_m = \pm\frac{\dot{\theta}_m^*}{3}\sum_{i=1}^{3}\left|\frac{\omega_i}{\omega_{a,i}^*}\right|, \tag{31}$$

where $\dot{\theta}_m^*$ is a reference joint velocity, ω_i is the component of angular velocity of IMUa, and $\omega_{a,i}^*$ is the same component of angular velocity under the velocity $\dot{\theta}_m^*$. The sign of $\dot{\theta}_m$ is uncertain and can be determined by using the differentiation of the joint positions.[14]

The estimation of the motion of joint l is not so straightforward. Before performing measurements, the orientation of IMUb relative to the end-effector's frame needs to be obtained. To solve this issue, one can rotate solely joint 1 while the others are locked into various configurations to obtain different orientations of the IMU. If the first joint is rotating, the angular acceleration of IMUb can be obtained from the IMU outputs and is denoted $\dot{\boldsymbol{\omega}}_b = [\dot{\omega}_{b,1}\ \dot{\omega}_{b,2}\ \dot{\omega}_{b,3}]^T$, the axis of the latter is

$$\mathbf{b} = \frac{1}{\|\dot{\boldsymbol{\omega}}\|}[\dot{\omega}_{b,1}\ \dot{\omega}_{b,2}\ \dot{\omega}_{b,3}]^T. \tag{32}$$

https://doi.org/10.1017/S0263574709990233 Published online by Cambridge University Press

Clearly, $\mathbf{b}$ is the direction vector of the first joint axis expressed in the IMU frame, i.e.,

$$ {}^{1}_{n}\mathbf{Q}\mathbf{R}_b\mathbf{b} = [0\ 0\ 1]^T, \tag{33} $$

where ${}^{1}_{n}\mathbf{Q}$ is the rotation matrix from the first frame to the end-effector frame (which is assumed to have the same orientation as the frame of joint n) and $\mathbf{R}_b$ represents the transformation from the end-effector frame to the IMUb frame. If there are k tests with different configurations from the second to the nth joint, one has

$$ \begin{aligned} &\left[{}^{1}_{n}\mathbf{Q}_1\mathbf{R}_b\mathbf{b}_1 \ \ldots\ {}^{1}_{n}\mathbf{Q}_k\mathbf{R}_b\mathbf{b}_k\right] \\ &\quad = [\,[0\ 0\ 1]^T \ \ldots\ [0\ 0\ 1]^T\,], \end{aligned} \tag{34} $$

which can be written as

$$ \mathbf{R}_b\mathbf{B} = \mathbf{M}, \tag{35} $$

where

$$ \mathbf{M} = \left[{}^{1}_{n}\mathbf{Q}_1^T[0\ 0\ 1]^T \ \ldots\ {}^{1}_{n}\mathbf{Q}_k^T[0\ 0\ 1]^T\right], \tag{36} $$

and

$$ \mathbf{B} = [\,\mathbf{b}_1 \ \ldots\ \mathbf{b}_k\,]. \tag{37} $$

Then, $\mathbf{R}_b$ can be solved from the previous equation, still using a LS estimate:

$$ \mathbf{R}_b = \mathbf{M}\mathbf{B}^T(\mathbf{B}\mathbf{B}^T)^{-1}. \tag{38} $$

When joint m and l are rotating simultaneously, the angular velocity and acceleration of link l with respect to frame l are respectively

$$ \begin{cases} \boldsymbol{\omega}_l = {}^{l}_{m}\mathbf{Q}\boldsymbol{\omega}_m + \dot{\theta}_l\mathbf{e}, \\ \dot{\boldsymbol{\omega}}_l = {}^{l}_{m}\mathbf{Q}\dot{\boldsymbol{\omega}}_m + {}^{l}_{m}\mathbf{Q}\boldsymbol{\omega}_m \times \dot{\theta}_l\mathbf{e} + \ddot{\theta}_l\mathbf{e}, \end{cases} \tag{39} $$

in which $\boldsymbol{\omega}_m = [0\ 0\ \dot{\theta}_m]^T$, $\dot{\boldsymbol{\omega}}_m = [0\ 0\ \ddot{\theta}_m]^T$, and $\mathbf{e} = [0\ 0\ 1]^T$. In particular, $\dot{\theta}_m$ and $\ddot{\theta}_m$ are obtained from Eqs. (30) and (31).

On the other hand, one has

$$ \begin{cases} \boldsymbol{\omega}_l = {}^{l}_{n}\mathbf{Q}\mathbf{R}_b\boldsymbol{\omega}_b\ , \\ \dot{\boldsymbol{\omega}}_l = {}^{l}_{n}\mathbf{Q}\mathbf{R}_b\dot{\boldsymbol{\omega}}_b\ , \end{cases} \tag{40} $$

where $\boldsymbol{\omega}_b$ is the output of the angular velocity of IMUb. Then, $\dot{\theta}_l$ and $\ddot{\theta}_l$ are easily found from Eqs. (39) and (40), namely,

$$ \dot{\theta}_l = \mathbf{e}^T\left({}^{l}_{n}\mathbf{Q}\mathbf{R}_b\boldsymbol{\omega}_b - {}^{l}_{m}\mathbf{Q}\boldsymbol{\omega}_m\right), \tag{41} $$

and

$$ \ddot{\theta}_l = \mathbf{e}^T\left({}^{l}_{n}\mathbf{Q}\mathbf{R}_b\dot{\boldsymbol{\omega}}_b - {}^{l}_{m}\mathbf{Q}\dot{\boldsymbol{\omega}}_m - {}^{l}_{m}\mathbf{Q}\boldsymbol{\omega}_m \times \dot{\theta}_l\mathbf{e}\right). \tag{42} $$

It should be noted that $\boldsymbol{\omega}_b$ in Eq. (41) also has a sign indetermination, which can be solved by referring to the previous time samples (i.e., the differentiation of joint angles).

Fig. 5. Experimental setup.

Finally, the proposed sequential identification approach is summarized in the following chart,

Dynamic model derivation
(Symbolic computation software)
⇓
Friction estimation with Eqs. (7–16)
(Single joint motion)
⇓
Gravity parameters $\boldsymbol{\pi}_g$ identification
with Eq. (19) (Single joint motion)
⇓
Inertial parameters $\boldsymbol{\pi}_r$ with Eq. (26)
(Two-joint motion and IMU measurement)

4. Experimental Verification

To validate the method proposed in this paper, experiments are conducted with two different simple setups: a one-joint manipulator with skewed joint axis and a two-joint planar manipulator. The experiment setup is illustrated in Fig. 5. The actuator is a Maxon F2140 motor with a 100 counts per revolution encoder and a 6:1 gearbox transmission. The joint axis is skew to the gravity vector with an angle of approximately 30°.

4.1. One-joint manipulator

In the case of a one-joint manipulator with skewed joint axis, the gravity effects have to be separated in the friction identification process. According to the previously described method, the joint is first controlled to follow a trajectory, part of which has a constant velocity; then, the joint follows the same motion in the reverse direction. Subsequently, the data collected from these two trajectories are processed using Eq. (15) to obtain τ_p. Illustrated in the first and the second plots of Fig. 6 are the joint torque profiles when the joint rotates in both directions. The estimated gravity torque is displayed in the third and last plot of Fig. 6.

Then, a LS estimation of the first-order mass moment of the link is formed by substituting the obtained data of the gravity torque into Eq. (12). The results are listed in Table I

https://doi.org/10.1017/S0263574709990233 Published online by Cambridge University Press

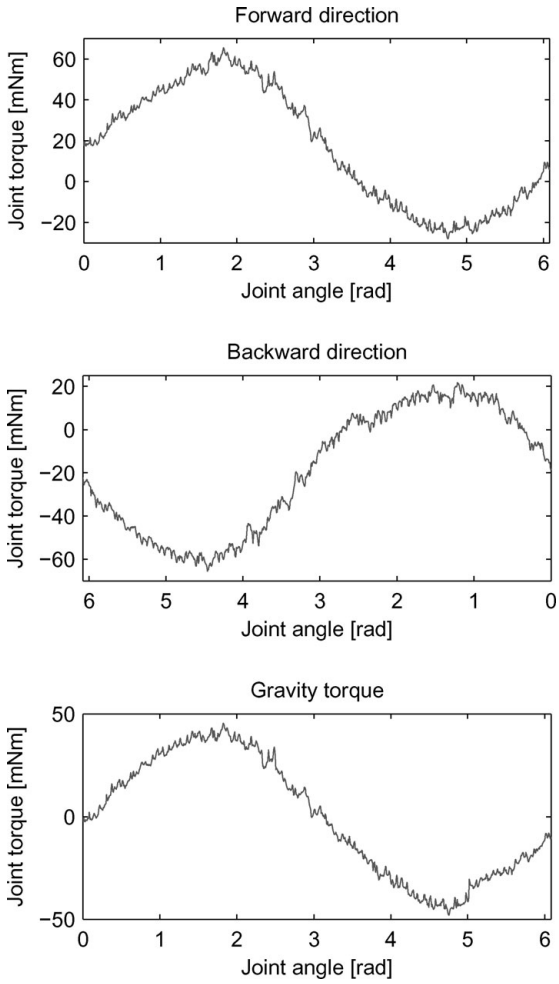

Fig. 6. τ_p identification.

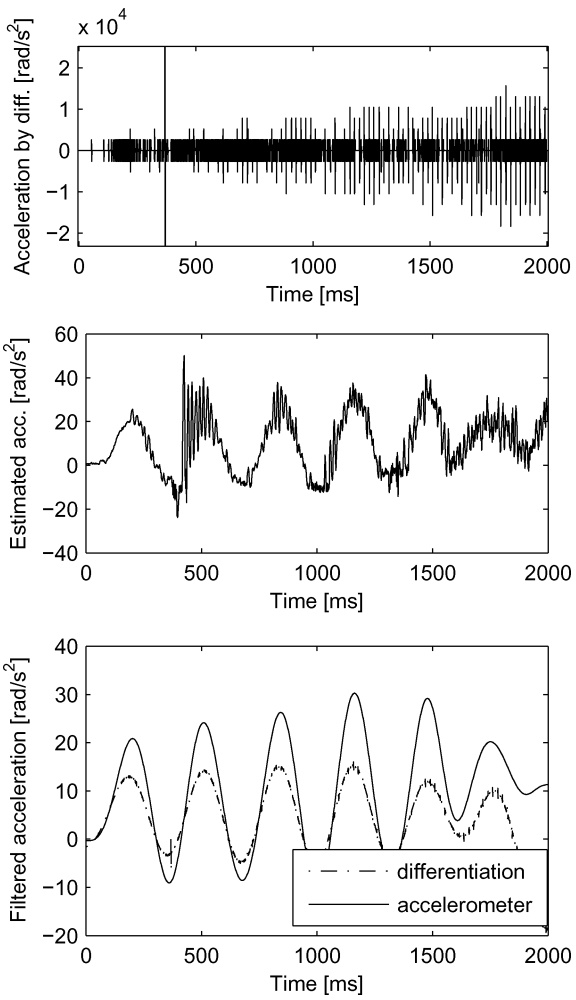

Fig. 7. Acceleration data to identify link inertia.

Table I. Identified gravity terms.

	Identified value (kg·m)	CAD value (kg·m)
mr_x	0.0090	0.0087
mr_y	0.0001	0

Table II. Identified link inertia (kg·m^2).

Test 1	Test 2	CAD
0.0034	0.0022	0.0019

and compared with CAD values. By comparing both values, the identification seems to provide reliable results.

After the identification of the gravity terms, experiments to obtain joint friction model are performed. Each time, the gravity-associated torque is subtracted from the joint torque to obtain only friction torque data. Then, the procedure detailed in Section 2.2.1 is followed to obtain the complete model of joint friction (examples will be provided in the next subsection).

Next, the inertia of the link is identified in two tests with different groups of data. In test #1, the joint velocity and acceleration is obtained by numerical differentiation of the encoder data, whereas, in test #2, an accelerometer is used to estimate the joint acceleration. Figure 7 illustrates some sampled data from these two tests. The first plot is the joint acceleration inferred from joint position data; the second one is based on accelerometers; the third plot displays the filtered signals which will be used in the identification. It can be seen that the acceleration data inferred from the joint encoder is very noisy due to discretization, resulting in large uncertainty in the identification process. The identification results from both tests are listed in Table II. The test using acceleration measurement performs much better than the numerical differentiation method in comparison with CAD value.

Using the identified inertia value and the joint friction model, the predicted actuator torque can be computed and compared with the actual torque which is inferred from the motor current. Figure 8 shows that the prediction of the joint torque matches well with the measurement data. The root mean square error (RMSE) of the actuator prediction is 8.16 (mNm). These results further validate the effectiveness of our approach.

Furthermore, the simultaneous identification with the proposed friction model using linear regression is investigated. However, the condition number of the regressor is found to be too large for the parameters to be identified properly. For instance, if m and l are chosen to be 10 and

https://doi.org/10.1017/S0263574709990233 Published online by Cambridge University Press

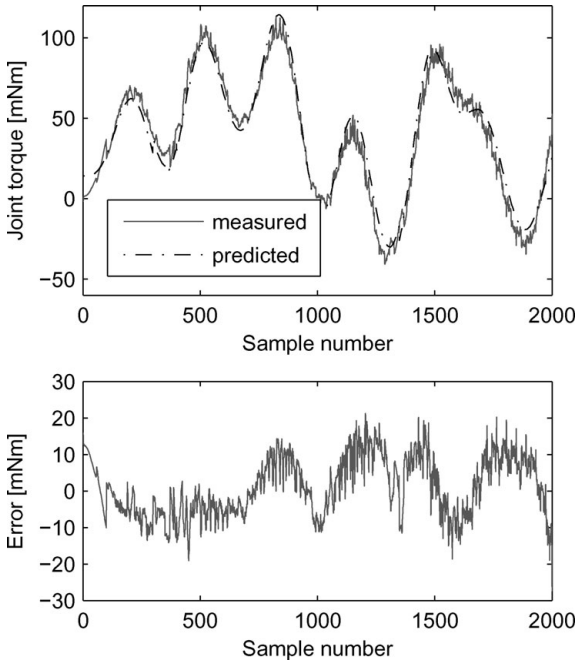

Fig. 8. Compare the predicted actuator torque with the actual torque.

Table III. Results of the simultaneous identification.

Link inertia	mr_x	mr_y	Coulomb	Viscous
0.0018	0.0095	−0.0004	0.0266	−0.0018

11 in Eqs. (7,9,10) for the friction model, there are elements such as $\theta^{10}\dot{\theta}^{11}$, $\theta^{9}\dot{\theta}^{10}$, etc. in the linear system, which result in an ill-conditioned regressor. Therefore, it is not practical to use the proposed friction model in the simultaneous identification approach. On the other hand, if a simple Coulomb-viscous friction model is used, a simultaneous identification can be conducted for comparison purposes. The identified parameters are reported in Table III. The prediction of the joint torque using these identified values also matches well with the measurement data and the root mean square error (RMSE) of the actuator prediction is 8.73 (mNm). However, the simultaneous approach yields a quite different set of parameters as compared to the estimated and CAD values presented in Tables I and II. Judging from the CAD values, it seems that the proposed approach performs better in this particular case, although CAD modeling errors might impact the precision. Nevertheless, it is clear that the choice of friction models yields a significant difference in the identification results. Therefore, large identification errors may result if the friction modeling is inaccurate.

4.2. Two-joint manipulator

Another experiment to identify the base parameters of a two-revolute joint planar manipulator as shown in Fig. 9 is conducted to further examine our proposed approach. The matrix $\mathbf{H}$ of Eq. (4) regarding this manipulator is

$$\mathbf{H} = \begin{bmatrix} \mathbf{A}_1 & \mathbf{A}_2 \end{bmatrix}, \tag{43}$$

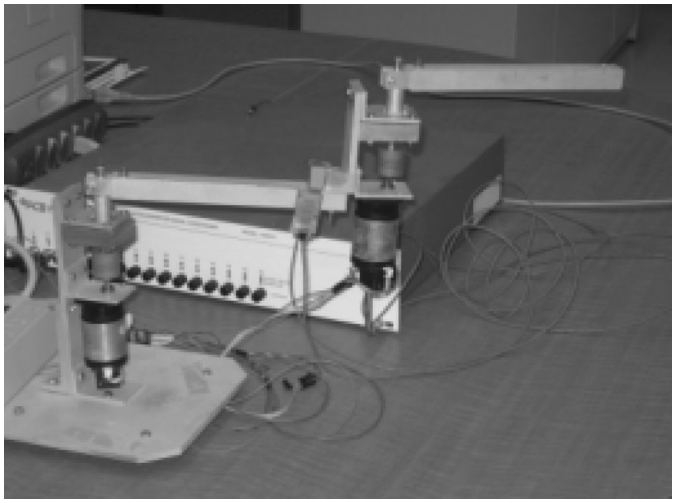

Fig. 9. Experimental setup of the two-joint manipulator.

where

$$\mathbf{A}_1 = \begin{bmatrix} \ddot{\theta}_1 & \ddot{\theta}_1 + \ddot{\theta}_2 & 0 \\ 0 & \ddot{\theta}_1 + \ddot{\theta}_2 & \ddot{\theta}_2 \end{bmatrix},$$

$$\mathbf{A}_2 = \begin{bmatrix} a_{21} & a_{22} \\ a_{23} & a_{24} \end{bmatrix},$$

with

$$a_{21} = -\left(2\,\dot{\theta}_1\dot{\theta}_2 + \dot{\theta}_2^2\right) l_1 \sin\theta_2 + (2\,\ddot{\theta}_1 + \ddot{\theta}_2) l_1 \cos\theta_2,$$

$$a_{22} = -\left(2\,\dot{\theta}_1\dot{\theta}_2 + \dot{\theta}_2^2\right) l_1 \cos\theta_2 - (2\,\ddot{\theta}_1 + \ddot{\theta}_2) l_1 \sin\theta_2,$$

$$a_{23} = \dot{\theta}_1^2 l_1 \sin\theta_2 + \ddot{\theta}_1 l_1 \cos\theta_2,$$

$$a_{24} = \dot{\theta}_1^2 l_1 \cos\theta_2 - \ddot{\theta}_1 l_1 \sin\theta_2.$$

The vector of base parameters is

$$\boldsymbol{\pi} = \begin{bmatrix} I_1^{zz} + N_1^2 I_{m,1} + m_2 l_1^2 \\ I_2^{zz} \\ N_2^2 I_{m,2} \\ m_2 r_2^x \\ m_2 r_2^y \end{bmatrix}, \tag{44}$$

where l_1 is the distance between the first and second joint. All the other parameters are explained in Section 2.1.

The identification of the joint friction is first performed. Since the manipulator is planar, the step to remove the gravity effects using Eqs. (12)–(16) is skipped. The friction models described by Eq. (7) for the two joints are obtained using Eqs. (8)–(11). In particular, m and l in Eqs. (8) and (10) are respectively set to 10 and 11 for both joints. Figure 10 shows the graphical representations of these two models corresponding to experimental data.

Proceeding with the identification, the next step, i.e., estimating gravity parameters described in Section 2.2.3, is again skipped since the manipulator is unaffected by the latter.

Next, the inertial parameters are identified using the method detailed in Section 2.2.4. Initially, data are collected when only the first joint is rotated while the second

https://doi.org/10.1017/S0263574709990233 Published online by Cambridge University Press

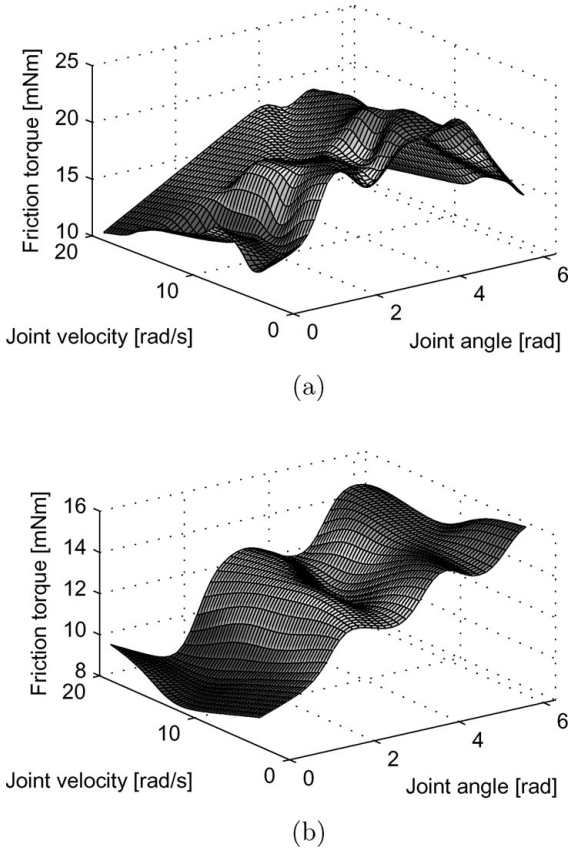

Fig. 10. Friction models of (a) the first joint, and (b) the second joint.

Table IV. Identified base parameters.

	Identified value	CAD value	Unit
π_1	0.0396	0.0388	(kg·m^2)
π_2	0.0021	0.0019	(kg·m^2)
π_4	0.0092	0.0087	(kg·m)
π_5	0.0001	0	(kg·m)

joint is fixed in different positions. Specifically, velocities and accelerations of the moving joint are estimated from accelerometers attaching to the end of the first link. The third element of vector $\boldsymbol{\pi}$ is given by the actuator manufacturer and substituted into the identification process. Finally, $\boldsymbol{\pi}$ is identified using Eq. (26), and the results for unknown parameters are listed in Table IV. It can be seen that the identification results are again close to the CAD values.

5. Conclusion

A systematic, sequential identification method to identify dynamic parameters of serial robots has been developed. The proposed method consists in the parametrization of friction as the function of both joint position and velocity, joint motion estimation by IMUs, and a sequential procedure to identify dynamic parameters. Experiments with this new joint friction modeling method and acceleration measurements show promising results when applied to the dynamic identification problem.

Acknowledgments

The financial support of Canada Foundation for Innovation (FCI) and Natural Sciences and Engineering Research Council (NSERC) of Canada are gracefully acknowledged.

References

1. B. Armstrong, "On finding exciting trajectories for identification experiments involving systems with nonlinear dynamics," *Int. J. Robot. Res.* **8**(6), 28–48 (1989).
2. B. Armstrong, O. Khatib and J. Burdick, "Explicit Dynamic Model and Inertial Parameters of the Puma 560 Arm," *Proceedings of the IEEE International Conference Robotics and Automation*, San Francisco, CA, USA (1986) pp. 510–518.
3. S. P. Chan, *Learning Friction Compensation in Robot Manipulators*, vol. 3. (Maui, HI, USA, 1993) pp. 2282–2287.
4. J. J. Craig, *Introduction to Robotics: Mechanics and Control*, 2nd ed. (Addison Wesley, Reading, Massachusetts, 1989).
5. M. Gautier and W. Khalil, "On the Identification of the Inertial Parameters of Robots," *Proceedings of the IEEE Conference on Decision and Control Including The Symposium on Adaptive Processes*, Austin, TX, USA (1988) pp. 2264–2269.
6. M. Gautier and W. Khalil, "Direct calculation of minimum set of inertial parameters of serial robots," *IEEE Trans. Robot. Autom.* **6**(3), 368–373 (1990).
7. M. Gautier and W. Khalil, "Exciting Trajectories for the Identification of Base Inertial Parameters of Robots," *Proceedings of the IEEE Conference on Decision and Control*, Brighton, England, UK (1992) pp. 494–499.
8. M. Gautier and C. Presse, "Sequential Identification of Base Parameters of Robots," *91 ICAR. Fifth International Conference on Advanced Robotics. Robots in Unstructured Environments (Cat. No.91TH0376-4)*, Pisa, Italy (1991) pp. 1105–1110.
9. P. K. Khosla, "Estimation of robot dynamics parameters: theory and application," *Int. J. Robot. Autom.* **3**(1), 35–41 (1988).
10. M. M. Olsen, J. Swevers and W. Verdonck, "Maximum likelihood identification of a dynamic robot model: Implementation issues," *Int. J. Robot. Res.* **21**(2), 89–96 (2002).
11. H. Olsson, K. J. Astrom, C. C. De Wit, M. Gafvert and P. Lischinsky, "Friction models and friction compensation," *Eur. J. Control* **4**(3), 176–195 (1998).
12. E. G. Papadopoulos and G. C. Chasparis, "Analysis and model-based control of servomechanisms with friction," *J. Dyn. Syst. Meas. Control Trans. ASME* **126**(4), 911–915 (2004).
13. C. Presse and M. Gautier, "New Criteria of Exciting Trajectories for Robot Identification," *Proceedings of the IEEE International Conference on Robotics and Automation*, vol. 3, Atlanta, GA, USA (1993) pp. 907–912.
14. Z. Qin, L. Baron and L. Birglen, "Robust design of all-accelerometer based inertial measurement unit," *J. Dyn. Syst. Meas. Control* **131**(3), (2009).
15. L. Sciavicco and B. Siciliano, *Modelling and Control of Robot Manipulators*. (Springer, London, 2000).
16. G. Seeger and W. Leonhard, "Estimation of Rigid Body Models for a Six-axis Manipulator with Geared Electric Drives," *Proceedings. 1989 IEEE International Conference on Robotics and Automation (Cat. No.89CH2750-8)*, Scottsdale, AZ, USA (1989) pp. 1690–1695.
17. J. Swevers, C. Ganseman, J. De Schutter and H. Van Brussel, "Experimental robot identification using optimised periodic trajectories," *Mech. Syst. Signal Process.* **10**(5), 561–577 (1996).
18. J. Swevers, W. Verdonck, B. Naumer, S. Pieters and E. Biber, "An experimental robot load identification method for industrial application," *Int. J. Robot. Res.* **21**(8), 701–712 (2002).
19. A. Zakharov and S. Halasz, "Genetic Algorithms based Identification Method for a Robot Arm," *IEEE International Symposium on Industrial Electronics*, Bled, Slovenia, **3**, 1014–1019 (1999).

https://doi.org/10.1017/S0263574709990233 Published online by Cambridge University Press